ACS OMEGA

Open Access

http://pubs.acs.org/journal/acsodf

Article

Ag Nanoparticle Layer on PEDOT:PSS with Optimized Energy Levels for Improving PM6:Y6-Based Organic Photovoltaics

Anderson E. X. Gavim, Yosthyn M. A. Florez, Patrick R. Zilz, Arandi G. Bezerra, Jr.,* Rafael E. de Góes, Paula C. Rodrigues, Wilson J. da Silva, Gregorio C. Faria, Paulo B. Miranda, Andreia G. Macedo, and Roberto M. Faria*

Cite This: *ACS Omega* 2025, 10, 37664−37673

Read Online

ACCESS | Metrics & More | Article Recommendations | Supporting Information

ABSTRACT: Recent advances in donor and acceptor molecules have significantly enhanced the efficiency and competitiveness of organic solar cells. However, optimizing the interfaces remains a critical issue in increasing the photovoltaic performance, mainly to reduce charge accumulation between the hole transport layers (HTLs) and the active layer. In this work, the interface between PM6:Y6 (active layer) and PEDOT:PSS (HTL) has been modified with silver nanoparticles (AgNPs). These AgNPs have been synthesized in anhydrous chlorobenzene by laser ablation synthesis in solution (LASiS). The choice of chlorobenzene as the medium for the synthesis of NPs by LASiS allows direct deposition onto the HTL. Measurements performed using steady-state current−voltage (J−V), Photo-CELIV, and current/voltage transient (TPC/TPV) revealed enhanced and reproducible photovoltaic parameters. The AgNPs also improve the device stability and can also be used on top of other HTLs, such as Br-2PACz. Theoretical analyses were performed by fitting an analytical model to the experimental data of photocurrent, which showed that the AgNP layer reduced bimolecular recombination losses. These findings suggest that the AgNP-modified interface of the PEDOT:PSS/active layer is a promising and versatile strategy to optimize interfacial properties, thus minimizing recombination losses and enhancing the efficiency, reproducibility, and stability of organic solar cells.

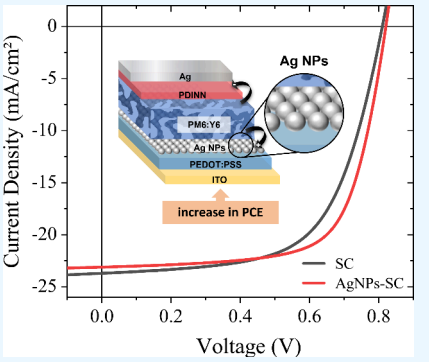

INTRODUCTION

The emergence of novel electron donor and acceptor molecules for bulk heterojunction organic solar cells (BHJ-OSCs), particularly nonfullerene Y6-type acceptors, has significantly advanced the field by pushing power conversion efficiencies (PCE) toward 20%, making these devices increasingly competitive.[1−5] A key breakthrough came with the efficient pairing of the PM6 donor with the Y6 acceptor, leading to substantial improvements in BHJ-OSC performance.[3] Furthermore, incorporating aliphatic amine-functionalized perylene-diimide (PDINN) as an electron injection layer successfully down-shifted the work function of the cathodes, thereby enhancing the interfacial contact with the active layer (AL).[6]

Despite these advances, issues persist due to the multilayer structure of BHJ-OSCs, particularly those related to interfacial energy misalignment, which restrict optimal device performance.[7−9] Additionally, the open-circuit voltage (V_{OC}) is constrained by the disparity between quasi-Fermi energy levels of holes,[10] which is often influenced by the alignment of energy levels at the anode interface. In an effort to address these challenges, numerous interface modifications have been explored to alter the performance and characteristics of BHJ-OSCs. Noteworthy among these efforts are hybrid graphene thin films[11,12] and oxide/metal nanoparticles,[13,14] which have been employed to enhance transparency, conductivity, and outdoor stability in organic photovoltaics.[15]

Thus, improving the hole-transporting layer (HTL) is critical to achieving better energy alignment and efficient charge extraction. Poly(3,4-ethylenedioxythiophene)-poly-(styrenesulfonate) (PEDOT:PSS) remains the most widely used polymeric HTL in BHJ-OSCs, demonstrating its versatility across various organic electronic devices.[16−18] To address the energy barriers present at the PEDOT:PSS layer interface, different approaches involving metallic nanoparticles have been applied, utilizing methods such as suspension processing,[19] ion implantation,[20] and aerosol techniques.[21] A clear illustration of this was presented by Brenes-Badilla et al., who demonstrated that PEDOT:PSS degraded upon exposure to air, causing a reduction in its HOMO energy level. However, the latter was restored after gold nanoparticles that were implanted into the PEDOT:PSS film, near the HTL/AL interface.[20] Additionally, studies have reported improvements

Received: May 7, 2025
Revised: August 4, 2025
Accepted: August 11, 2025
Published: August 15, 2025

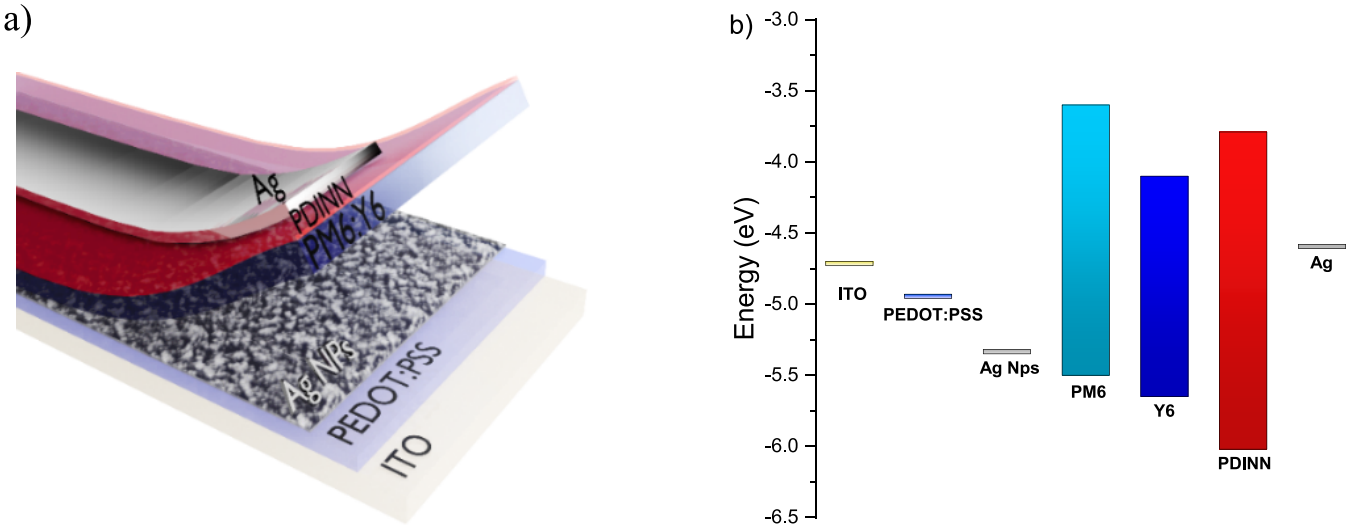

Figure 1. (a) Device geometry and (b) energy level diagram for devices with the structure ITO/PEDOT:PSS/AgNPs/PM6:Y6/PDINN/Ag.

in the PCE of organic solar cells due to the plasmonic effects generated by metal nanoparticles embedded within PEDOT:PSS.[22,23] For example, Ganeshan et al.[24] demonstrated that incorporating size-controlled silver nanoparticles (AgNPs) into the PEDOT:PSS layer can significantly enhance the power conversion efficiency (PCE) of fullerene-based OSCs from 7.90 to 9.45%. This was attributed to the plasmonic scattering effects of AgNPs, which increased the light absorption and charge collection at the HTL/AL interface.

In this study, the PEDOT:PSS/active layer interface has been modified with AgNPs. This procedure increased the PCE measured from ITO/PEDOT:PSS/PM6:Y6/PDINN/Ag devices. These AgNPs have been synthesized by the laser ablation synthesis in solution (LASiS) technique, where bulk metals are ablated by a laser beam in an aqueous or organic medium.[13,25] This top-down LASiS route eliminates the precursor chemistry, ligand exchange, and high-temperature reduction steps that are inherent to wet-chemical syntheses. Such procedure yields bare metallic AgNPs that are completely surfactant-free and with their intrinsic electronic properties.[24] Because the ablation is performed directly in anhydrous chlorobenzene, no solvent-exchange or drying sequence is required, thus avoiding water uptake by PEDOT:PSS and preventing ionic or surfactant contamination of the HTL/active-layer interface. The AgNP dispersion is dropped onto the rotating substrate and, in <1 min, forms a uniform interlayer without impacting the PEDOT:PSS layer.

This approach aimed to adjust the energy alignment at the HTL-AL interface through a straightforward deposition technique. Subsequently, a comprehensive analysis of device behavior was performed by fitting the current−voltage (J−V) characteristics using two models: (i) the traditional solar-cell equivalent-circuit equation[26] and (ii) an analytical expression assuming second-order recombination kinetics.[27] Ultimately, the incorporation of AgNPs also resulted in more consistent device fabrication, reducing variability in key parameters such as series and parallel resistances (R_s and R_{sh}), fill factor (FF), and PCE.

EXPERIMENTAL SECTION

Bulk heterojunction organic solar cells (BHJ-OSCs) are assembled layer by layer, in the following sequence: deposition of the hole transport layer (HTL) on ITO-coated glass; deposition of a nanostructured film of donor and acceptor polymers; deposition of an electron transport layer (ETL); and finally, evaporation of a metal electrode (cathode). In this work, we built two similar devices: ITO/PEDOT:PSS/PM6:Y6/PDINN/Ag, designated by SC, and ITO/PEDOT:PSS/AgNPs/PM6:Y6/PDINN/Ag, referred to as AgNPs-SC. Each step of the device manufacturing procedure (materials, the silver nanoparticle synthesis, and the device structure) is described in the Supporting Information, along with complementary characterization measurements (AFM, UV−vis spectroscopy, transient photovoltage (TPV), transient photocurrent (TPC), and Photo-CELIV). The surface potential images have been acquired by the Kelvin probe technique (Bruker Dimension Icon probe microscope): ITO (4.7 eV), PEDOT:PSS (4.95 eV), AgNPs (5.35 eV), and Ag (4.5 eV). HOMO values from the literature are PM6 (5.45 eV),[28] Y6 (5.65 eV),[3] and PDINN (6.02 eV).[29]

RESULTS AND DISCUSSION

Figure 1a presents the device geometry highlighting the localization of the AgNP layer. Figure 1b presents the energy level diagram for the OSCs built with the PEDOT:PSS/AgNPs as the HTL. The surface potential images (Figure S6) pointed out a work function of 4.94 eV for PEDOT:PSS, in accordance with values in the literature[30,31] and the manufacturer, while the PEDOT:PSS/AgNP film presented a higher work function of 5.35 eV. Therefore, this modified HTL presents a proper energy level alignment to extract holes from the HOMO level from copolymers that have been used as donors in OSCs, such as PM6 (HOMO level ≈ 5.45 eV)[32,33] and PTB7-Th (HOMO level ≈ 5.4 eV).[34] Therefore, as indicated by the kelvin probe analyses, the AgNP layer improved both the interface smoothness (see also Section 3.1) and the energy alignment (Figure 1b) with the active layer, providing a lower energy barrier for the process of hole extraction. This reduces hole accumulation at the AL/HTL interface, reducing the probability of e−h recombination in that region.

3.1. Morphology Analysis by AFM. AFM images acquired using a high-resolution tip pointed out that the AgNPs deposited on glass in static mode (see preparation details in the Supporting Information) form aggregates with

https://doi.org/10.1021/acsomega.5c04247
ACS Omega 2025, 10, 37664−37673

size dimensions on the order of 50 nm (Figure 2a). However, the height and phase image acquired from the films deposited

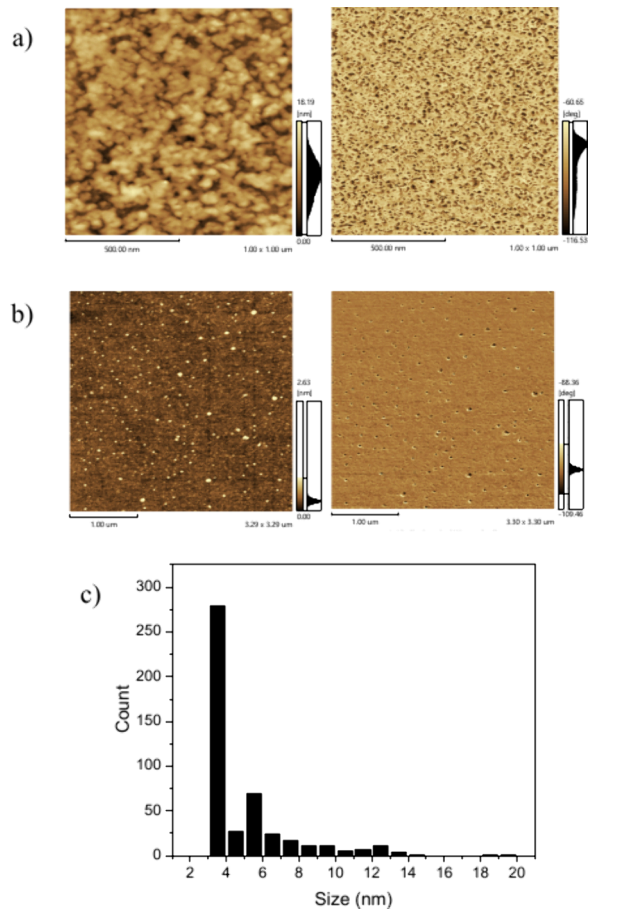

Figure 2. Height and phase AFM images acquired from AgNP film on glass prepared using the spin coating in (a) static mode, (b) dynamic mode, and (c) the size distribution profile from the image in (b).

by spin coating in dynamic mode (substrate upon rotation before the dropping) led to more isolated AgNPs and yielded the real (multimodal) size distribution on the order of 3, 5, and ≈12 nm (Figure 2b). Elongated structures with lengths of ca. 100 nm and diameters of ca. 10 nm have also been observed, but in minor amounts.

The histogram (Figure 2c) reveals that particles below 12 nm dominate the population; this is compatible with dynamic light scattering (DLS) measurements of the NP suspension (Figure S3) that shows an average size of the AgNPs in suspension of ≈7.8 nm with a predominant population around 4 nm; this prevalence of smaller AgNPs should help them settle into shallow depressions on PEDOT:PSS and suppress clustering, favoring the formation of a uniform, compact overlayer. Considering that the AgNPs present a more uniform and nonaggregated distribution along the surface when the film is prepared in dynamic mode, this procedure was adopted to produce AgNP films onto the PEDOT:PSS surface.

Figure 3a–c presents the AFM height images of different batches of the pristine PEDOT:PSS film (thickness of 38.09 ± 0.99 nm, obtained by AFM, Figure S4a), which exhibits an amorphous landscape characterized by a root-mean-square roughness (Rq) of 1.51 ± 0.27 nm. In contrast, the corresponding images of the PEDOT:PSS/AgNPs (thickness of 46.16 ± 0.96 nm, obtained by AFM, Figure S4b) shown in Figure 3d–f reveals a uniform dispersion of AgNPs distributed across the polymer surface, with the roughness attenuated to 0.86 ± 0.11 nm. The ≈43% decline in Rq is probably due to the nanoparticles settling into and filling subnanometric troughs, given that chlorobenzene is not expected to appreciably swell or dissolve the underlying PEDOT:PSS matrix. Such planarization removes nanoscopic asperities that otherwise can act as charge-trapping pockets and local electric-field hot spots at the PEDOT:PSS/active-layer junction. Therefore, this smoother HTL surface, both topographically and electronically, favors more efficient carrier extraction and diminished recombination. Complementary energy-dispersive X-ray spectroscopy (EDS) elemental mapping (Figure S5) of AgNPs dispersed in a polystyrene matrix (10 wt % of AgNPs) confirms that Ag-rich regions are devoid of oxygen, demonstrating preservation of the metallic state throughout film formation (in an inert atmosphere) and handling (in air). Because LASiS produces surfactant and ligand-free AgNPs directly in anhydrous chlorobenzene, these bare particles can be deposited onto the PEDOT:PSS film without inducing polymer swelling or leaving ionic residues, concomitantly flattening the surface and up-shifting its work function from 4.95 to 5.35 eV (Figure S6), a level of interfacial optimization that traditional wet-chemical routes struggle to match.

Moreover, Figure S7 shows the transmittance spectra acquired from the resulting films. Similar transmittance spectra have been obtained from these films, with a minor decrease at some regions, and thus, with a minor impact in the amount of light reaching the active layer with the additional AgNP layer.

3.2. *J*–*V*, TPC and TPV Transients, and Photo-CELIV Measurements. As stated by the AFM and kelvin probe analysis, the deposited layer of AgNPs on top of the PEDOT:PSS layer contributes to aligning the HOMO of the HTL with the HOMO of the active layer, which facilitates the collection of holes by the anode. To probe this, first *J*–*V* measurements of both BHJ-OSC devices, SC and AgNPs-SC, in the dark and under illumination (AM1.5G condition) are shown in Figure 4a and Figure 4b, respectively. In the dark, the diode responses of both devices are similar, and the distinction between them emerges in favor of the AgNPs-SC device only for voltages above 0.8 V, probably due to the decrease in the series resistance. The presence of AgNPs did not change the diode behavior in the region in which the *J*–*V* curve is dominated by injection of charge carriers and effects of space charge. On the other hand, under illumination, a noticeable improvement in device performance when the AgNP layer is added is shown in Figure 4b. Solar-cell parameter values, obtained from 12 devices of each type (SC and AgNPs-SC), are shown in Figure 5 and corroborate that the addition of AgNPs improves the device performance. Figure 5 also shows that the dispersions of the FF, R_s, R_{sh}, and PCE decrease considerably when depositing the nanoparticles at the PEDOT:PSS-active layer interface. This shows that nanoparticles improve reproducibility in organic solar-cell manufacturing. The average values of these parameters are shown in Table 1.

J–*V* results under illumination show that the AgNPs deposited at the PEDOT:PSS-active layer interface leads to a small decrease in J_{SC} but contribute to a slight increase in open-circuit voltage. The slight decrease in short-circuit current is due to the equivalent decrease in absorbance of the AgNPs-SC device, as shown in Figure S7; this is further

https://doi.org/10.1021/acsomega.5c04247
ACS Omega 2025, 10, 37664–37673

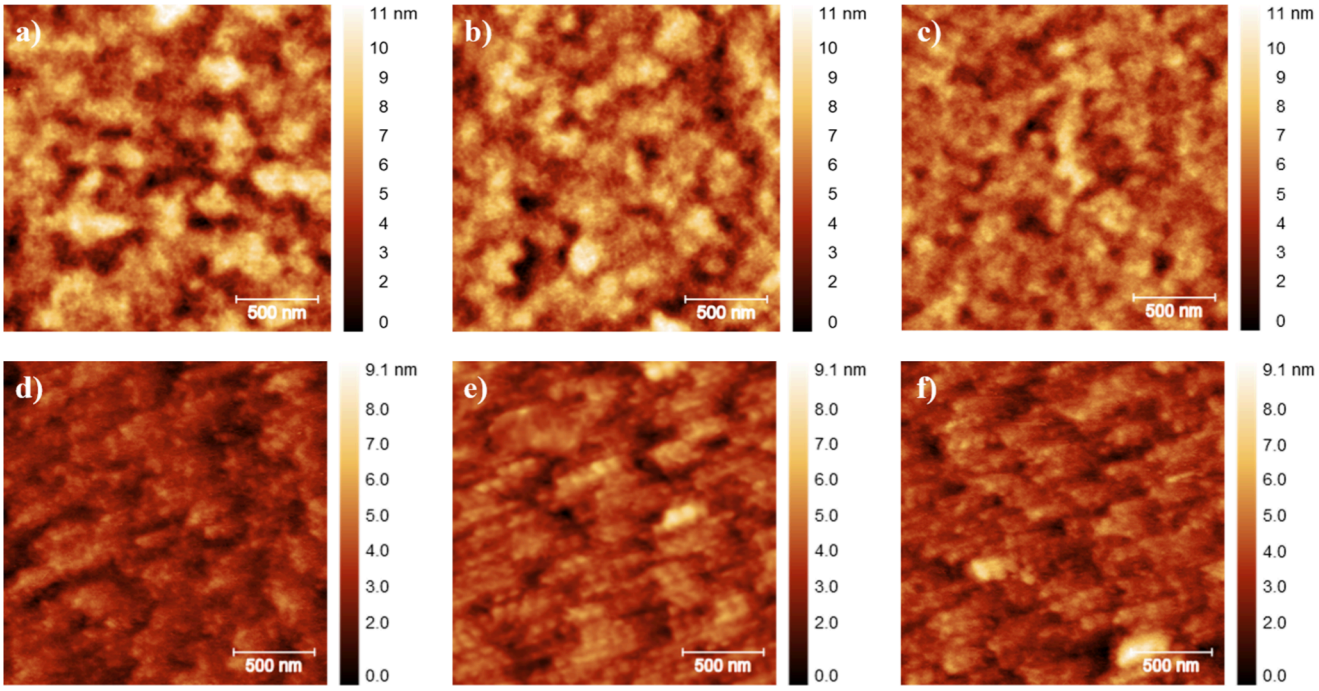

Figure 3. AFM height images for different batch films of PEDOT:PSS (a–c) and PEDOT:PSS/AgNPs (d–f) deposited on glass/ITO.

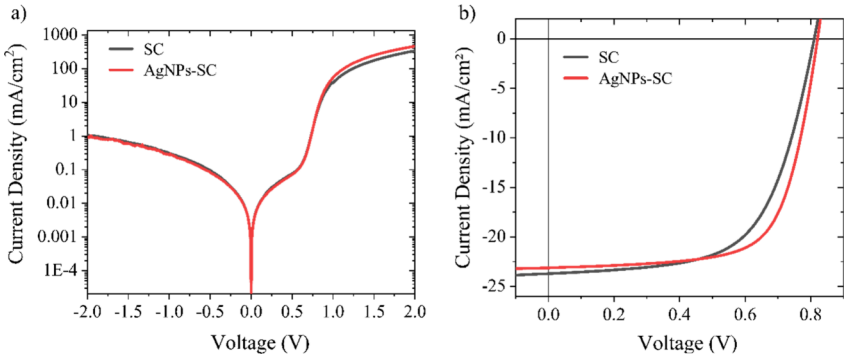

Figure 4. (a) $J-V$ curves acquired in the dark, and (b) $J-V$ curves acquired under illumination at the AM1.5G condition from the ITO/X/PM6:Y6/PDINN/Ag devices, where X = PEDOT:PSS or PEDOT:PSS/AgNPs.

confirmed by TMM simulations of the experimental cells that shows that the simulated J_{SC}, obtained from the exciton generation rate ($G(x)$) (Figure S8), decreases ≈3.5%, which is compatible with the ≈3% decrease of the experimental J_{SC}. Because J_{SC} is (slightly) reduced by the deposition of AgNPs, the absorption enhancement from a possible plasmonic effect due to an evanescent field can be ruled out, since there was no significant increase in the electric current near the J_{SC} point. The most significant improvement occurs in the fill factor; not only the FF value shows a robust increase, but also a considerable reduction in the dispersion of values for the 12 devices measured, with respect to the devices without AgNPs. This reduction in FF dispersion for devices incorporating AgNPs is consistent with the fill factor's relationship to the shape of the $J-V$ curve and intrinsic device properties, such as charge mobility and recombination rate,[27] reflecting a more reproducible device structure and fabrication. In contrast, both J_{SC} and the maximum extracted power remain more variable due to their heightened susceptibility to measurement conditions (e.g., fluctuations in illumination or device positioning), rather than the fabrication process itself. Similar improvement was observed in the series and parallel resistances, which shows the close relationship between these resistances and the fill factor. The significant improvement of the FF can be explained by the convergence between the HOMOs of the HTL and the active layer donor,[35] which mitigates the accumulation of charge carriers at the interface. Additionally, it is worth emphasizing that the accumulation of charge carriers at internal interfaces of photovoltaic devices strengthens nongeminate recombination and distorts the electric field within the active layer. The ≈8% relative increase in PCE, is compatible with other works reported in literature with modifications at the HTL/Al interface for similar nonfullerene systems, such as the ≈6% relative increase in PCE for systems with PEDOT:PSS modified with sulfonated graphene[36] and gold nano double cones.[37] This makes the increase in PCE from ≈12 to ≈13% in devices with the AgNP layer an interesting, straightforward, and remarkable method to enhance both the PCE and reproducibility of such devices. Finally, it is worth highlighting that the efficiency of the control device is within the same range as those reported in the literature for lower molecular mass PM6,[38−40] since the

https://doi.org/10.1021/acsomega.5c04247
ACS Omega 2025, 10, 37664−37673

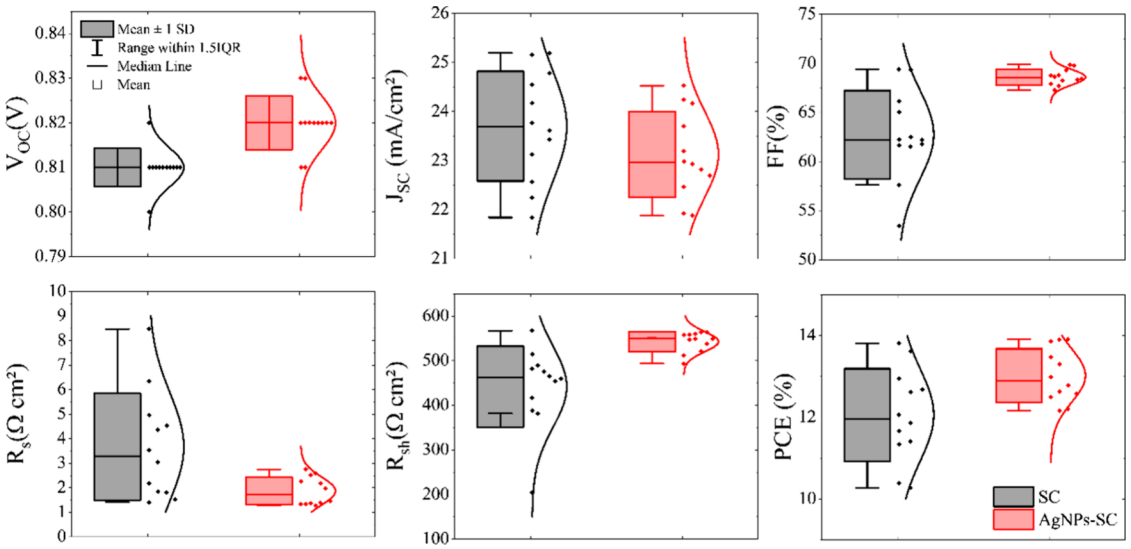

Figure 5. Photovoltaic parameters obtained for the ITO/X/PM6:Y6/PDINN/Ag devices, where X = PEDOT:PSS or PEDOT:PSS/AgNPs. The parameters R_s and R_{sh} were extracted by fitting each cell's $J-V$ curve with the solar-cell equivalent-circuit equation.[13]

Table 1. Average Photovoltaic Parameters

HTL	V_{OC} (V)	J_{SC} (mA/cm²)	FF (%)	R_s (Ω·cm²)	R_{sh} (Ω·cm²)	PCE (%)
SC	0.81	23.7	62.8	3.67	441.7	12.0
AgNPs-SC	0.82	23.1	68.6	1.87	542.7	13.0

molecular mass of PM6 is an important parameter that influences the performance of high-efficiency OSCs, as shown in Figure S9 and Table S1.

Additionally, to show the versatility of the AgNP layer on top of other types of HTL to optimize the HTL/AL interface, tests were performed with Br-2PACz molecule as HTL, a known substitute to PEDOT:PSS.[41] The Br-2PACz monolayer has a work function (5.21 eV, Figure S11b) that already matches the PM6 HOMO (5.45 eV) more closely than PEDOT:PSS (4.95 eV). After spin-coating AgNPs (5.35 eV) on Br-2PACz, the energy offset between the HTL and the HOMO of PM6 is further reduced from 0.24 to ≈0.10 eV and the rms roughness drops from 3.85 to 0.88 nm (Figure S11a). These changes translate into the performance trends shown in Figure S10, where the J_{SC} rises from ≈23.8 to ≈24.5 mA cm^{-2}, and the average PCE increases from ≈13.5 to ≈14.2%. Because Br-2PACz already affords good energetic alignment, this smaller (≈ 5%) relative gain compared with the PEDOT:PSS case is attributed mainly to the interfacial smoothing supplied by the AgNP layer, which improves the charge collection efficiency and overcompensates the small optical loss introduced by the AgNP layer.

To further understand the charge dynamics in the cells with PEDOT:PSS, transient measurements were performed; Figure 6 shows transient photocurrent (TPC) and transient photovoltage (TPV) measurements carried out with SC and AgNPs-SC devices. The TPC decay curves of both devices showed that decay times were similar, so it can be inferred that the deposition of AgNPs into the device apparently does not influence the charge extraction mechanism. This is further confirmed by a log−log analysis of J_{SC} versus light intensity plot (Figure S12a) that gives α = 0.945 for SC and 0.942 for AgNPs-SC, values close to unity that confirm efficient photogeneration/extraction and negligible bimolecular losses under short-circuit conditions. TPV measurements show an increase in the decay time of the AgNPs-SC device in comparison to the SC one, indicating that the deposition of the nanoparticles increases the recombination time. This is consistent with the proposed reduction in charge accumulation at the HTL-active layer interface, which decreases recombination and leads to a higher FF. This is further confirmed by a semilog V_{OC} vs light intensity plot (Figure S12b) that yields slopes of 1.39 kT/q for SC and 1.22 kT/q for AgNPs-SC,

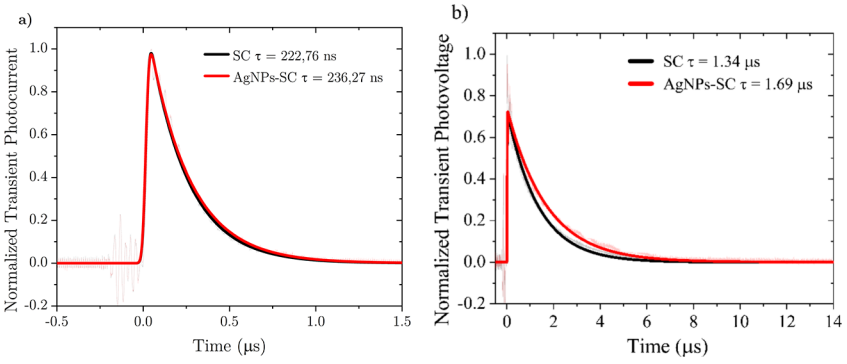

Figure 6. (a) TPC and (b) TPV response for ITO/X/PM6:Y6/PDINN/Ag devices, where X = PEDOT:PSS or PEDOT:PSS/AgNPs.

https://doi.org/10.1021/acsomega.5c04247
ACS Omega 2025, 10, 37664−37673

evidencing a marked reduction in recombination losses when the AgNP interlayer is present. This longer TPV decay, together with the higher FF, is fully consistent with the smoother surface observed by AFM images, suggesting reduced trapping at the HTL-active layer interface; this confirms that the morphological leveling and energy alignment produced by the AgNP interlayer directly reduces interfacial recombination.

To further investigate the impact of AgNPs on charge extraction and mobility, Photo-CELIV measurements (Figure 7) were performed on both devices and analyzed using eq 1 from Bange et al.[42] This equation incorporates a correction for CELIV transients, enabling the determination of mobility even under conditions of high charge density and assuming that Langevin recombination dominates. The obtained values are understood as an average value of the mobilities of electrons and holes ($\mu = \sqrt{\mu_e \mu_h}$).

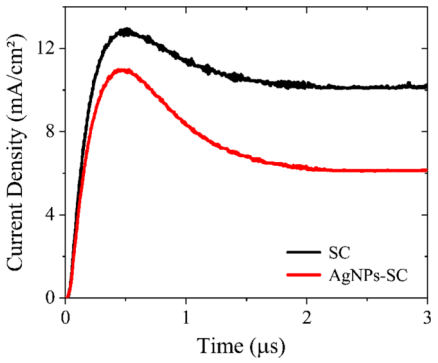

Figure 7. Photo-CELIV response of the ITO/X/PM6:Y6/PDINN/Ag cells, where X = PEDOT:PSS or PEDOT:PSS/AgNPs.

$$\mu = \frac{2d^2}{U' t_{max}^2}\left(0.860e^{-0.486\Delta j/j(0)} - 0.525e^{0.0077\Delta j/j(0)}\right) \quad (1)$$

The calculated values for the mobilities are 4.89×10^{-4} and 5.12×10^{-4} cm^2 V^{-1} s^{-1} for devices without and with AgNPs, respectively. This slight increase can be explained by the decrease in the charge accumulated at the HTL-active layer interface, due to the intermediate energy step interposed by the AgNPs, thus facilitating the flow of holes throughout the device and increasing the hole collection rate by the ITO electrode. That is, the enhanced hole flux between the active layer and the ITO electrode is compatible with the increased effective charge carrier mobility.

3.3. *J*–*V* Analysis by a Photocurrent Model. For a more detailed analysis of the role played by the deposition of AgNPs at the HTL-active layer interface, we adjusted the *J*–*V* curves under illumination by eq 2, which is a theoretical expression derived by Amorim et al.[27] that includes the effect of second-order recombination. It is well known that in BHJ-OSCs, excitons generated by absorbed photons decay into a donor–acceptor charge transfer state (CTS), which may or may not dissociate into free charges: positive in the donor phase and negative in the acceptor phase. The recombination of a CTS pair (geminate recombination) is measured by the $(1 - P)$ factor, where P is the probability of dissociation of CTS. After being dissociated, the photocarriers migrate toward the electrodes where they will be collected, generating the device's electric current. However, during this migration, recombination between charge carriers originating from different CTS can occur, resulting in the called nongeminate recombination. In the Amorim model, the nongeminate recombination between the photocarriers is assumed to be of second-order kinetics, obeying a Langevin recombination mechanism. The Langevin recombination coefficient is $\gamma_L\left(=\frac{e\mu}{\varepsilon\varepsilon_0}\right)$, and in BHJ-OSCs it is well accepted that the recombination coefficient γ is reduced relative to the Langevin coefficient by a certain factor.[43−45]

$$J(V) = \frac{2eG_{ct}PL}{\theta_o}\left(1 - \frac{V}{V_{bi}}\right)^2\left[\sqrt{1 + \frac{\theta_o}{\left(1 - \frac{V}{V_{bi}}\right)^2}} - 1\right] \quad (2)$$

In eq 2, G_{ct} is the generation rate of CT states, V_{bi} is the built-in voltage, and θ_o is the physical parameter, defined by eq 3:

$$\theta_o = \frac{G_{ct}PL^4(1 - P)\gamma_L}{(\mu V_{bi})^2} \quad (3)$$

Figure 8a shows the fittings of SC and AgNPs-SC photocurrents extracted from Figure 4b by eq 2. However, the model ceases to be reliable for values close to the V_{OC}, since the derivation of eq 2 does not take into account the contribution of the diffusion current, which is dominant when

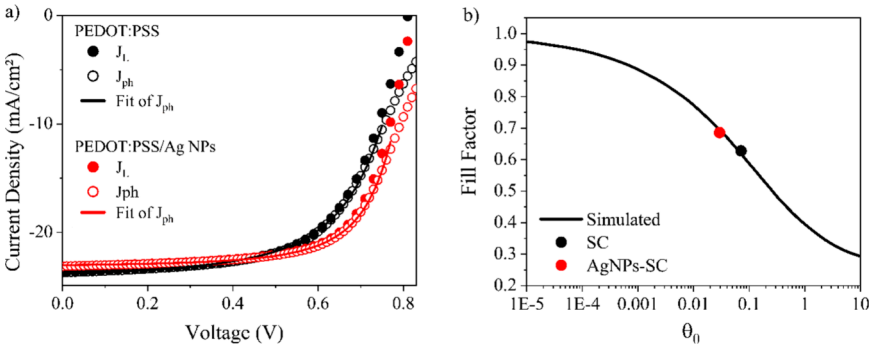

Figure 8. (a) Fits to eq 2 for the *J*–*V* results of Figure 4b. J_{ph} is the photocurrent defined by the difference between current in light condition (J_L) and the current in dark condition (J_D). (b) Calculated dependence of FF on the parameter θ_0, from the Amorim model. The black and red points indicate the experimentally measured FF values for devices with PEDOT:PSS and PEDOT:PSS/AgNPs as hole transport layers.

https://doi.org/10.1021/acsomega.5c04247
ACS Omega 2025, 10, 37664−37673

Table 2. Summary of Charge Generation, Transport, and Recombination Parameters

device	θ_o	μ (10^{-4} cm^2 V^{-1} s^{-1})	GP (10^{22} cm^{-3} s^{-1})	P	γ (10^{-11} cm^3 s^{-1})
SC	0.072	4.89	1.50	0.85	7.57
AgNPs-SC	0.029	5.12	1.45	0.93	3.58

the device's internal field tends to zero. For the fittings, GP and $(1 - P)$ were used as adjustable parameters. The mobilities were obtained from the Photo-CELIV measurements, $V_{bi} = V_{OC}$, and $\gamma_L\left(=\frac{e\mu}{\varepsilon\varepsilon_0}\right)$ is calculated using 3.5 for the dielectric constant. The values of the fitted parameters (GP and P) are exhibited in Table 2, together with θ_o, $\gamma = (1 - P)\gamma_L$, and μ that were obtained from measured quantities as described above. The saturation currents calculated by equation $J_{sat} = eGPL$, using the GP values of Table 2, show excellent agreement with the values recorded in Figure 4b. Note that the largest change in those parameters occurs for the recombination rate γ, a factor of 2 lower for AgNPs-SC, consistent with our interpretation that the reduced barrier for hole extraction at the HTL-active layer interface decreases nongeminate charge recombination in these devices.

The relationship that exists between the θ_o parameter and the FF was discussed by Bartesaghi et al., who defined θ_o as the ratio between the extraction rate and the recombination rate of photocarriers in BHJ-OSCs.[46] Based on simulated $J-V$ curves for a large range of FFs, they showed that FF follows a logistic type of curve (S-shaped), in which, in a monolog scale, FF is high for small values of θ_o and low for large values of θ_o. In ref 46, the authors showed that results collected from 15 devices with different combinations of donor and acceptor molecules obey such FF-θ_o pattern. Amorim et al.[27] have derived an FF(θ_o) implicit analytical expression using eq 2 and making the derivative of $J(V)\cdot V$ vanish at the maximum power point:

$$\mathrm{FF}(\theta_o) = \frac{v(1-v)^3}{(2v-1)(\sqrt{1+\theta_o})}, \text{ with } \theta_o = \frac{(1-v)^3(3v-1)}{(2v-1)^2} \quad (4)$$

where $v = \frac{V_{max}}{V_{bi}}$ is the voltage at the maximum power point. The "universal FF(θ_o) curve" is depicted in Figure 8b, and it was shown that the points of the measured FF for the SC and AgNP devices vs the respective θ_o values obtained from the fitting parameters are located nearly perfectly on the FF(θ_o) curve. This suggests that the conditions for the Amorin model (balanced electron and hole mobilities, uniform internal electric field, negligible contribution of diffusion currents, and assuming second-order recombination) are valid for our devices, at least for voltages up to the maximum power point.

3.4. Stability Tests. The stability of organic photovoltaic devices under atmosphere conditions is a critical parameter, particularly due to the known susceptibility of PEDOT:PSS to moisture, as it is a hygroscopic material.[47,48] The stability of our devices was then investigated under the ISOS-T-2 protocol,[49,50] where we subjected unencapsulated cells to 200 h of thermal cycling between 25 and 85 °C in the dark and in open air at ≈32% RH. Such conditions better approximate real-world, field-relevant stresses.

As depicted in Figure 9, AgNPs-SC demonstrates a markedly slower efficiency decay than the reference SC device, with the time required to reach 80% of the initial power conversion

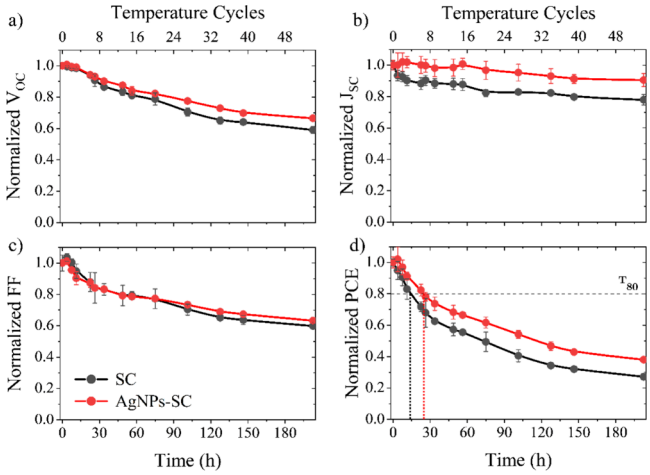

Figure 9. Normalized evolution of (a) V_{OC}, (b) J_{SC}, (c) FF, and (d) PCE for SC and AgNPs-SC devices, during the thermal cycling test (temperature ramping from 25 to 85 °C, during 3.75 h cycles, with RH of 32%) according to the ISOS-T-2 protocol.[49,50]

efficiency (T_{80}) extending from ≈14.5 h for SC to ≈24 h for AgNPs-SC, and the 50% threshold (T_{50}) shifting from ≈73 to ≈116 h. Both the open-circuit voltage and the J_{SC} are better preserved in the AgNPs-SC cells throughout the test, confirming that the metallic interlayer mitigates humidity- and temperature-driven degradation at the PEDOT:PSS/active-layer interface.

For comparison, a shorter but harsher high-humidity test (65–85% RH, 3 h, unencapsulated, Figure S13) likewise shows that devices containing AgNPs retain a larger fraction of their initial performance (≈46 versus ≈36% for SC), again underscoring the protective role of the nanoparticle layer under moisture exposure.

The superior performance of the AgNPs-SC can be attributed to several factors. First, the AgNP layer appears to mitigate moisture-induced degradation at the PEDOT:PSS interface, which is often a critical site for performance loss. The presence of the AgNP layer can help diminish the known moisture-assisted decohesion of the PEDOT:PSS layer at the AL interface,[51] reducing moisture ingress and thereby preserving interfacial properties while minimizing the formation of trap states at the interface. Additionally, since V_{OC} is inherently dependent on the difference between the quasi-Fermi levels of the electrodes,[52] which in turn is influenced by the energy levels of materials at the interface, and PEDOT:PSS is known to experience shifts in its work function when exposed to moisture,[53] the AgNP layer may help delay these effects at the HTL/AL interface.

Furthermore, while metallic nanoparticles can be susceptible to oxidative processes that may decrease interfacial stability, the AgNPs employed in this study were synthesized via the LASiS technique in chlorobenzene. This method produces nanoparticles with inherently stable surface chemistry due to the absence of chemical precursors and stabilizing agents, which often contribute to oxidative degradation.[54,55] This

https://doi.org/10.1021/acsomega.5c04247
ACS Omega 2025, 10, 37664−37673

characteristic is likely to reduce their susceptibility to oxidation under ambient conditions and temperature stress.

Lastly, considering the strategic positioning of the AgNPs at the HTL/AL interface rather than embedded within the PEDOT:PSS bulk, the potential for significant diffusion into the layer is expected to be minimal. To verify this, cells were fabricated and stored under dark conditions in a nitrogen glovebox environment (≈3 ppm of O_2 and moisture) for 3200 h. These conditions enable the observation of natural aging processes, including potential diffusion phenomena. Figure S14 shows the normalized photovoltaic parameters after this period for both device types, revealing that cells with and without the AgNP layer retained ≈88% of their initial PCE, which is consistent with shelf life data reported for similarly structured cells stored in the dark under an inert atmosphere.[56,57] This result indicates no significant difference between SC and AgNPs-SC devices, and thus similar aging-related processes under these conditions, even with the presence of the AgNP layer. Overall, these findings suggest that the incorporation of the AgNP layer not only enhances device performance and moisture stability but also does not introduce additional long-term degradation pathways, supporting its viability for stable, high-performance organic photovoltaic devices.

4. CONCLUSIONS

This study demonstrates that the AgNP-modified PEDOT:PSS layer resulted in an enhanced photovoltaic performance from PM6:Y6-based organic photovoltaic, arising from improved energy level alignment at the HTL/active layer interface. The AgNP layer led to an 8% increase in PCE and an improved V_{OC} due to better HOMO alignment. TPV measurements confirmed that the AgNP layer reduces recombination losses, leading to an increased FF. Additionally, AgNPs improved the reproducibility of the devices, as reflected by reduced variability in key parameters, including FF, R_s, and R_{sh}. They also provide a protective effect against humidity and thermally induced degradation of the active layer-HTL interface, improving the device stability.

Further insights from a second-order recombination kinetics model highlighted the role of AgNPs in decreasing non-geminate recombination at the HTL-active layer interface, creating a more favorable charge transport environment. Furthermore, we have also shown that the use of AgNPs on top of the HTL is a simple and versatile strategy that can be applied to different HTL layers, as long as there is a match of the donor HOMO to the AgNPs' work function. These findings suggest that AgNPs provide an effective means of optimizing interfacial properties, which minimize recombination losses and enhance both efficiency, reproducibility and stability of organic solar cells.

■ ASSOCIATED CONTENT

Supporting Information

The Supporting Information is available free of charge at https://pubs.acs.org/doi/10.1021/acsomega.5c04247.

Materials and device fabrication details, additional device characterizations, additional morphological (AFM) and spectroscopic (UV−Vis) characterizations, and basic concepts about transient measurements (PDF)

■ AUTHOR INFORMATION

Corresponding Authors

Arandi G. Bezerra, Jr. − *PPGFA, Federal University of Technology, Curitiba, Paraná 80230-901, PR, Brazil;* orcid.org/0000-0002-5145-5131; Email: arandi@utfpr.edu.br

Roberto M. Faria − *Sao Carlos Physics Institute, University of Sao Paulo, São Carlos, SP 13566-590, Brazil; PPGFA, Federal University of Technology, Curitiba, Paraná 80230-901, PR, Brazil; PPGQ, Federal University of Technology, Curitiba, Paraná 81280-340, PR, Brazil;* orcid.org/0000-0002-0088-442X; Email: faria@ifsc.usp.br

Authors

Anderson E. X. Gavim − *Sao Carlos Physics Institute, University of Sao Paulo, São Carlos, SP 13566-590, Brazil;* orcid.org/0000-0001-6189-6267

Yosthyn M. A. Florez − *Sao Carlos Physics Institute, University of Sao Paulo, São Carlos, SP 13566-590, Brazil*

Patrick R. Zilz − *CPGEI, Federal University of Technology, Curitiba, Paraná 80230-901, PR, Brazil*

Rafael E. de Góes − *PPGFA, Federal University of Technology, Curitiba, Paraná 80230-901, PR, Brazil*

Paula C. Rodrigues − *PPGQ, Federal University of Technology, Curitiba, Paraná 81280-340, PR, Brazil;* orcid.org/0000-0002-9712-6149

Wilson J. da Silva − *CPGEI, Federal University of Technology, Curitiba, Paraná 80230-901, PR, Brazil*

Gregorio C. Faria − *Sao Carlos Physics Institute, University of Sao Paulo, São Carlos, SP 13566-590, Brazil;* orcid.org/0000-0001-6138-8473

Paulo B. Miranda − *Sao Carlos Physics Institute, University of Sao Paulo, São Carlos, SP 13566-590, Brazil;* orcid.org/0000-0002-2890-0268

Andreia G. Macedo − *PPGFA, Federal University of Technology, Curitiba, Paraná 80230-901, PR, Brazil;* orcid.org/0000-0002-3114-9954

Complete contact information is available at: https://pubs.acs.org/10.1021/acsomega.5c04247

Author Contributions

Anderson Emanuel Ximim Gavim: conceptualization, investigation, formal analysis, validation, and writing—original draft. Yosthyn Manuel Ariza Florez: investigation and formal analysis. Patrick Rangel Zilz: investigation and validation. Arandi Ginane Bezerra Jr: investigation and writing—review and editing. Rafael Eleodoro de Góes: investigation. Paula Cristina Rodrigues: writing—review and editing. Gregorio Couto Faria: formal analysis and writing—review and editing. Wilson José da Silva: writing—review and editing. Paulo Barbeitas Miranda: conceptualization, methodology, supervision, and writing—review and editing. Andreia Gerniski Macedo: investigation, formal analysis, conceptualization, and writing—review and editing. Roberto Mendonça Faria: conceptualization, methodology, supervision, and writing—review and editing.

Funding

The Article Processing Charge for the publication of this research was funded by the Coordenacao de Aperfeicoamento de Pessoal de Nivel Superior (CAPES), Brazil (ROR identifier: 00x0ma614).

Notes

The authors declare no competing financial interest.

■ ACKNOWLEDGMENTS

This work was financed by Conselho Nacional de Desenvolvimento Científico e Tecnológico (CNPq, 128040/2022-0, 315772/2020-4, and 309907/2021-7), CNPq BRICS-STI (442239/2017-3), Instituto Nacional de Eletrônica Orgânica (INEO) (CNPq − 465572/2014-6), Fundação de Amparo à Pesquisa do Estado de São Paulo (FAPESP, 2014/50869-6, 2022/15666-3), and Fundação Araucária (NAPI Eletrônica Orgânica). The authors acknowledge J.V. Barbosas Jr and E.H.S Rosa for initial device characterizations, LAMAQ − UTFPR for AFM measurements and LMA-IQ-UNESP for the SEM facilities used in this work.

■ REFERENCES

(1) Li, S.; He, C.; Chen, T.; Zheng, J.; Sun, R.; Fang, J.; Chen, Y.; Pan, Y.; Yan, K.; Li, C.-Z.; Shi, M.; Zuo, L.; Ma, C.-Q.; Min, J.; Liu, Y.; Chen, H. Refined molecular microstructure and optimized carrier management of multicomponent organic photovoltaics toward 19.3% certified efficiency, Energy. *Environ. Sci.* **2023**, *16*, 2262−2273.

(2) Fu, J.; Fong, P. W. K.; Liu, H.; Huang, C. S.; Lu, X.; Lu, S.; Abdelsamie, M.; Kodalle, T.; Sutter-Fella, C. M.; Yang, Y.; Li, G. 19.31% binary organic solar cell and low non-radiative recombination enabled by non-monotonic intermediate state transition. *Nat. Commun.* **2023**, *14*, 1760.

(3) Yuan, J.; Zhang, Y.; Zhou, L.; Zhang, G.; Yip, H.-L.; Lau, T.-K.; Lu, X.; Zhu, C.; Peng, H.; Johnson, P. A.; Leclerc, M.; Cao, Y.; Ulanski, J.; Li, Y.; Zou, Y. Single-Junction Organic Solar Cell with over 15% Efficiency Using Fused-Ring Acceptor with Electron-Deficient Core. *Joule* **2019**, *3*, 1140−1151.

(4) Chen, C.; Wang, L.; Xia, W.; Qiu, K.; Guo, C.; Gan, Z.; Zhou, J.; Sun, Y.; Liu, D.; Li, W.; Wang, T. Molecular interaction induced dual fibrils towards organic solar cells with certified efficiency over 20%. *Nat. Commun.* **2024**, *15*, 6865.

(5) Chen, H.; Huang, Y.; Zhang, R.; Mou, H.; Ding, J.; Zhou, J.; Wang, Z.; Li, H.; Chen, W.; Zhu, J.; Cheng, Q.; Gu, H.; Wu, X.; Zhang, T.; Wang, Y.; Zhu, H.; Xie, Z.; Gao, F.; Li, Y.; Li, Y. Organic solar cells with 20.82% efficiency and high tolerance of active layer thickness through crystallization sequence manipulation. *Nat. Mater.* **2025**, *24*, 444.

(6) Yao, J.; Qiu, B.; Zhang, Z.-G.; Xue, L.; Wang, R.; Zhang, C.; Chen, S.; Zhou, Q.; Sun, C.; Yang, C.; Xiao, M.; Meng, L.; Li, Y. Cathode engineering with perylene-diimide interlayer enabling over 17% efficiency single-junction organic solar cells. *Nat. Commun.* **2020**, *11*, 2726.

(7) Tang, H.; Bai, Y.; Zhao, H.; Qin, X.; Hu, Z.; Zhou, C.; Huang, F.; Cao, Y. Interface Engineering for Highly Efficient Organic Solar Cells. *Adv. Mater.* **2024**, *36*, No. 2212236.

(8) Wang, C.; Li, W.; Zeng, Q.; Liu, X.; Fahlman, M.; Bao, Q. Organic Semiconductor Interfaces and Their Effects in Organic Solar Cells†. *Chin. J. Chem.* **2023**, *41*, 3792−3805.

(9) Gusain, A.; Faria, R. M.; Miranda, P. B. Polymer solar cells-interfacial processes related to performance issues. *Front. Chem.* **2019**, *7*, 61.

(10) Yip, H.-L.; Jen, A. K.-Y. Recent advances in solution-processed interfacial materials for efficient and stable polymer solar cells, Energy. *Environ. Sci.* **2012**, *5*, 5994−6011.

(11) Beliatis, M. J.; Gandhi, K. K.; Rozanski, L. J.; Rhodes, R.; McCafferty, L.; Alenezi, M. R.; Alshammari, A. S.; Mills, C. A.; Jayawardena, K. D. G. I.; Henley, S. J.; Silva, S. R. P. Hybrid Graphene-Metal Oxide Solution Processed Electron Transport Layers for Large Area High-Performance Organic Photovoltaics. *Adv. Mater.* **2014**, *26*, 2078−2083.

(12) Christopholi, L. P.; da Cunha, M. R. P.; Spada, E. R.; Gavim, A. E. X.; Hadano, F. S.; da Silva, W. J.; Rodrigues, P. C.; Macedo, A. G.; Faria, R. M.; de Deus, J. F. Reduced graphene oxide and perylene derivative nanohybrid as multifunctional interlayer for organic solar cells. *Synth. Met.* **2020**, *269*, No. 116552.

(13) Gavim, A. E. X.; da Cunha, M. R. P.; Spada, E. R.; Machado, T. N.; Hadano, F. S.; Ginane Bezerra, A.; Herwig Schreiner, W.; Rodrigues, P. C.; bin Mohd Yusoff, A. R.; Macedo, A. G.; Faria, R. M.; da Silva, W. J. Water-suspended MoO3 nanoparticles prepared by LASIS and fast processing as thin film by ultrasonic spray deposition. *Sol. Energy Mater. Sol. Cells* **2019**, *200*, No. 109986.

(14) Pegg, L.-J.; Hatton, R. A. Nanoscale Geometric Electric Field Enhancement in Organic Photovoltaics. *ACS Nano* **2012**, *6*, 4722−4730.

(15) Kim, S.; Lee, E.; Lee, Y.; Kim, J.; Park, B.; Jang, S.-Y.; Jeong, S.; Oh, J.; Lee, M. S.; Kang, H.; Lee, K. Interface Engineering for Fabricating Semitransparent and Flexible Window-Film-Type Organic Solar Cells. *ACS Appl. Mater. Interfaces* **2020**, *12*, 26232−26238.

(16) Santos, G. H.; Gavim, A. A.; Silva, R. F.; Rodrigues, P. C.; Kamikawachi, R. C.; de Deus, J. F.; Macedo, A. G. Roll-to-roll processed PEDOT:PSS thin films: application in flexible electrochromic devices. *J. Mater. Sci.: Mater. Electron.* **2016**, *27*, 11072.

(17) Yamamoto, N. A. D.; Lima, L. F.; Perdomo, R. E.; Valaski, R.; Calil, V. L.; Macedo, A. G.; Cremona, M.; Roman, L. S. Modification of PEDOT:PSS anode buffer layer with HFA for flexible polymer solar cells. *Chem. Phys. Lett.* **2013**, *572*, 73−77.

(18) Faria, G. C.; Duong, D. T.; Salleo, A. On the transient response of organic electrochemical transistors. *Org. Electron* **2017**, *45*, 215−221.

(19) Qian, M.; Li, M.; Shi, X.-B.; Ma, H.; Wang, Z.-K.; Liao, L.-S. Planar perovskite solar cells with 15.75% power conversion efficiency by cathode and anode interfacial modification. *J. Mater. Chem. A Mater.* **2015**, *3*, 13533−13539.

(20) Brenes-Badilla, D.; Coutinho, D. J.; Amorim, D. R. B.; Faria, R. M.; Salvadori, M. C. Reversing an S-kink effect caused by interface degradation in organic solar cells through gold ion implantation in the PEDOT:PSS layer. *J. Appl. Phys.* **2018**, *123*, No. 155502.

(21) Jung, K.; Song, H.-J.; Lee, G.; Ko, Y.; Ahn, K.; Choi, H.; Kim, J. Y.; Ha, K.; Song, J.; Lee, J.-K.; Lee, C.; Choi, M. Plasmonic Organic Solar Cells Employing Nanobump Assembly via Aerosol-Derived Nanoparticles. *ACS Nano* **2014**, *8*, 2590−2601.

(22) Ko, S.-J.; Choi, H.; Lee, W.; Kim, T.; Lee, B. R.; Jung, J.-W.; Jeong, J.-R.; Song, M. H.; Lee, J. C.; Woo, H. Y.; Kim, J. Y. Highly efficient plasmonic organic optoelectronic devices based on a conducting polymer electrode incorporated with silver nanoparticles, Energy. *Environ. Sci.* **2013**, *6*, 1949−1955.

(23) Rivera-Taco, J.; Castro-Beltrán, R.; Maldonado, J.-L.; Álvarez-Martínez, J.; Barreiro-Argüelles, D.; Gaspar, J. A.; Gutiérrez-Juárez, G. The Role of Silver Nanoparticles in the Hole Transport Layer in Organic Solar Cells Based on PBDB-T:ITIC. *J. Electron. Mater.* **2021**, *50*, 4118−4127.

(24) Ganeshan, D.; Chen, S. C.; Yin, Z.; Zheng, Q. An anode buffer layer with size-controlled Ag nanoparticles for polymer solar cells with improved efficiencies. *RSC Adv.* **2015**, *5*, 16153−16161.

(25) Rosa, E. H. D. S.; Gavim, A. E.; de Araújo, F. L.; de Morais, A.; de Freitas, J. N.; Bezerra, A. G. Jr.; Macedo, A. G.; da Silva, W. J.; Nogueira, A. F. Scavenger effect of Au NPs to stabilize the excess of TFSI− from Spiro-OMeTAD layer. *Sol. Energy Mater. Sol. Cells* **2024**, *264*, No. 112600.

(26) Nelson, J. A. *The Physics of Solar Cells*; PUBLISHED BY IMPERIAL COLLEGE PRESS AND DISTRIBUTED BY World Scientific Publishing Company: 2003. .

(27) Amorim, D. R. B.; Coutinho, D. J.; Miranda, P. B.; Faria, R. M. Analytical Model for Photocurrent in Organic Solar Cells as a Function of the Charge-Transport Figure of Merit Including Second-Order Recombination. *Phys. Rev. Appl.* **2020**, *14*, 34046.

(28) Zhang, H.; Yao, H.; Hou, J.; Zhu, J.; Zhang, J.; Li, W.; Yu, R.; Gao, B.; Zhang, S.; Hou, J. Over 14% Efficiency in Organic Solar Cells Enabled by Chlorinated Nonfullerene Small-Molecule Acceptors. *Adv. Mater.* **2018**, *30*, No. 1800613.

https://doi.org/10.1021/acsomega.5c04247
ACS Omega 2025, 10, 37664−37673

(29) Zhang, Z.-G.; Qi, B.; Jin, Z.; Chi, D.; Qi, Z.; Li, Y.; Wang, J. Perylene diimides: a thickness-insensitive cathode interlayer for high performance polymer solar cells. *Energy Environ. Sci.* **2014**, *7*, 1966.
(30) Cook, J. H.; Al-Attar, H. A.; Monkman, A. P. Effect of PEDOT−PSS resistivity and work function on PLED performance. *Org. Electron* **2014**, *15*, 245−250.
(31) Meng, Y.; Hu, Z.; Ai, N.; Jiang, Z.; Wang, J.; Peng, J.; Cao, Y. Improving the Stability of Bulk Heterojunction Solar Cells by Incorporating pH-Neutral PEDOT:PSS as the Hole Transport Layer. *ACS Appl. Mater. Interfaces* **2014**, *6*, 5122−5129.
(32) Li, X.; Ma, R.; Liu, T.; Xiao, Y.; Chai, G.; Lu, X.; Yan, H.; Li, Y. Fine-tuning HOMO energy levels between PM6 and PBDB-T polymer donors via ternary copolymerization. *Sci. China Chem.* **2020**, *63*, 1256−1261.
(33) Wang, Y.; Fan, Q.; Guo, X.; Li, W.; Guo, B.; Su, W.; Ou, X.; Zhang, M. High-performance nonfullerene polymer solar cells based on a fluorinated wide bandgap copolymer with a high open-circuit voltage of 1.04 V. *J. Mater. Chem. A Mater.* **2017**, *5*, 22180−22185.
(34) Khlaifia, D.; Alimi, K. PTB7-Th /Non-fullerene acceptors for organic solar cells. *Synth. Met.* **2022**, *291*, No. 117189.
(35) Zhou, X.; Dong, X.; Liu, Y.; Wang, W.; Wei, W.; Chen, J.; Liu, T.; Zhou, Y. Effect of Wetting Surfactants on the Work Function of PEDOT:PSS for Organic Solar Cells. *ACS Appl. Energy Mater.* **2022**, *5*, 3766−3772.
(36) Pei, S.; Xiong, X.; Zhong, W.; Xue, X.; Zhang, M.; Hao, T.; Zhang, Y.; Liu, F.; Zhu, L. Highly Efficient Organic Solar Cells Enabled by the Incorporation of a Sulfonated Graphene Doped PEDOT:PSS Interlayer. *ACS Appl. Mater. Interfaces* **2022**, *14*, 34814−34821.
(37) Zhao, Y.; Wu, Y.; Song, J.; Zeng, J.; Dai, Z.; Li, H.; Quan, J.; Zong, Q.; Liang, G.; Lin, B.; Zheng, Z.; Guo, L.; Liu, S.; Wang, H.; Zhou, E.; Li, Z. An effective universal ternary complex hole transport material enabled by intermolecular interactions for polymer solar cells. *Colloids Surf. A Physicochem Eng. Asp* **2025**, *710*, No. 136270.
(38) Adil, M. A.; Memon, W. A.; Zhang, J.; Iqbal, M. J.; Yang, C.; Wang, Y.; Zou, W.; Wei, Z. Utilizing Ternary Strategy to Reduce the Influence of Polymer Batch-to-Batch Variation in Organic Solar Cells. *Sol. RRL* **2022**, *6*, No. 2101083.
(39) Yoon, S.; Schopp, N.; Choi, D. G.; Wakidi, H.; Ding, K.; Ade, H.; Vezin, H.; Reddy, G. N. M.; Nguyen, T. Q. Influences of Metal Electrodes on Stability of Non-Fullerene Acceptor-Based Organic Photovoltaics. *Adv. Funct. Mater.* **2024**, *34*, No. 2308618.
(40) Yoon, S.; Reyes-Suárez, B.; Pham, S. T.; Vezin, H.; Tobon, Y. A.; Lee, M.; Mugiraneza, S.; Kim, B. M.; Oide, M. Y. T.; Yoo, S.; Lee, S.; Wang, S. H.; Collins, S. M.; Bates, C. M.; Park, Y.; Kim, B. S.; Manjunatha Reddy, G. N.; Nguyen, T. Q. Molecular Cross-Linking Enhances Stability of Non-Fullerene Acceptor Organic Photovoltaics. *ACS Energy Lett.* **2025**, *10*, 541−551.
(41) Lin, Y.; Magomedov, A.; Firdaus, Y.; Kaltsas, D.; El-Labban, A.; Faber, H.; Naphade, D. R.; Yengel, E.; Zheng, X.; Yarali, E.; Chaturvedi, N.; Loganathan, K.; Gkeka, D.; AlShammari, S. H.; Bakr, O. M.; Laquai, F.; Tsetseris, L.; Getautis, V.; Anthopoulos, T. D. 18.4% Organic Solar Cells Using a High Ionization Energy Self-Assembled Monolayer as Hole-Extraction Interlayer. *ChemSusChem* **2021**, *14*, 3569−3578.
(42) Bange, S.; Schubert, M.; Neher, D. Charge mobility determination by current extraction under linear increasing voltages: Case of nonequilibrium charges and field-dependent mobilities. *Phys. Rev. B: Condens. Matter Mater. Phys.* **2010**, *81*, No. 035209.
(43) Lakhwani, G.; Rao, A.; Friend, R. H. Bimolecular Recombination in Organic Photovoltaics. *Annu. Rev. Phys. Chem.* **2014**, *65*, 557−581.
(44) Burke, T. M.; Sweetnam, S.; Vandewal, K.; McGehee, M. D. Beyond Langevin Recombination: How Equilibrium Between Free Carriers and Charge Transfer States Determines the Open-Circuit Voltage of Organic Solar Cells. *Adv. Energy Mater.* **2015**, *5*, No. 1500123.
(45) Liu, Y.; Zojer, K.; Lassen, B.; Kjelstrup-Hansen, J.; Rubahn, H.-G.; Madsen, M. Role of the Charge-Transfer State in Reduced Langevin Recombination in Organic Solar Cells: A Theoretical Study. *J. Phys. Chem. C* **2015**, *119*, 26588−26597.
(46) Bartesaghi, D.; Pérez, I. D. C.; Kniepert, J.; Roland, S.; Turbiez, M.; Neher, D.; Koster, L. J. A. Competition between recombination and extraction of free charges determines the fill factor of organic solar cells. *Nat. Commun.* **2015**, *6*, 7083.
(47) Liu, L.; Wu, L.; Yang, H.; Ge, H.; Xie, J.; Cao, K.; Cheng, G.; Chen, S. Conductivity and Stability Enhancement of PEDOT:PSS Electrodes via Facile Doping of Sodium 3-Methylsalicylate for Highly Efficient Flexible Organic Light-Emitting Diodes. *ACS Appl. Mater. Interfaces* **2022**, *14*, 1615−1625.
(48) Xu, B.; Gopalan, S. A.; Gopalan, A. I.; Muthuchamy, N.; Lee, K. P.; Lee, J. S.; Jiang, Y.; Lee, S. W.; Kim, S. W.; Kim, J. S.; Jeong, H. M.; Kwon, J. B.; Bae, J. H.; Kang, S. W. Functional solid additive modified PEDOT:PSS as an anode buffer layer for enhanced photovoltaic performance and stability in polymer solar cells. *Sci. Rep.* **2017**, *7*, 45079.
(49) Reese, M. O.; Gevorgyan, S. A.; Jørgensen, M.; Bundgaard, E.; Kurtz, S. R.; Ginley, D. S.; Olson, D. C.; Lloyd, M. T.; Morvillo, P.; Katz, E. A.; Elschner, A.; Haillant, O.; Currier, T. R.; Shrotriya, V.; Hermenau, M.; Riede, M.; Kirov, K. R.; Trimmel, G.; Rath, T.; Inganäs, O.; Zhang, F.; Andersson, M.; Tvingstedt, K.; Lira-Cantu, M.; Laird, D.; McGuiness, C.; Gowrisanker, S.; Pannone, M.; Xiao, M.; Hauch, J.; Steim, R.; DeLongchamp, D. M.; Rösch, R.; Hoppe, H.; Espinosa, N.; Urbina, A.; Yaman-Uzunoglu, G.; Bonekamp, J.-B.; van Breemen, A. J. J. M.; Girotto, C.; Voroshazi, E.; Krebs, F. C. Consensus stability testing protocols for organic photovoltaic materials and devices. *Sol. Energy Mater. Sol. Cells* **2011**, *95*, 1253−1267.
(50) Florez, Y. M. A. Células solares de terceira geração: estudo do efeito da degradação nos parâmetros fotovoltaicos. Doctoral dissertation, Universidade de São Paulo, 2023. .
(51) Dupont, S. R.; Novoa, F.; Voroshazi, E.; Dauskardt, R. H. Decohesion kinetics of PEDOT:PSS conducting polymer films. *Adv. Funct Mater.* **2014**, *24*, 1325−1332.
(52) Qi, B.; Wang, J. Open-circuit voltage in organic solar cells. *J. Mater. Chem.* **2012**, *22*, 24315−24325.
(53) Wachsmuth, J.; Distler, A.; Deribew, D.; Salvador, M.; Brabec, C. J.; Egelhaaf, H. J. Overcoming Moisture-Induced Degradation in Organic Solar Cells. *Adv. Eng. Mater.* **2023**, *25*, No. 2300595.
(54) Scaramuzza, S.; Agnoli, S.; Amendola, V. Metastable alloy nanoparticles, metal-oxide nanocrescents and nanoshells generated by laser ablation in liquid solution: Influence of the chemical environment on structure and composition. *Phys. Chem. Chem. Phys.* **2015**, *17*, 28076−28087.
(55) Amendola, V.; Meneghetti, M. Laser ablation synthesis in solution and size manipulation of noble metal nanoparticles. *Phys. Chem. Chem. Phys.* **2009**, *11*, 3805−3821.
(56) Ghasemi, M.; Balar, N.; Peng, Z.; Hu, H.; Qin, Y.; Kim, T.; Rech, J. J.; Bidwell, M.; Mask, W.; McCulloch, I.; You, W.; Amassian, A.; Risko, C.; O'Connor, B. T.; Ade, H. A molecular interaction−diffusion framework for predicting organic solar cell stability. *Nat. Mater.* **2021**, *20*, 525−532.
(57) Tu, S.; Lin, X.; Xiao, L.; Zhen, H.; Wang, W.; Ling, Q. Boosting the overall stability of organic solar cells by crosslinking vinyl-functionalized polymer derived from PM6. *Mater. Chem. Front* **2022**, *6*, 1150−1160.

https://doi.org/10.1021/acsomega.5c04247
ACS Omega 2025, 10, 37664−37673